AGU PUBLICATIONS

JGR

Journal of Geophysical Research: Space Physics

RESEARCH ARTICLE
10.1002/2014JA020461

Key Points:
- Near ±E hemispheric flanks, the magnetic field is directed equatorward
- Hemispheric asymmetry is suggested to be transported tailward from terminator
- Tailward plasma acceleration is most efficient near the +E hemispheric flank

Correspondence to:
Z. J. Rong,
rongzhaojin@mail.iggcas.ac.cn

Citation:
Rong, Z. J., S. Barabash, Y. Futaana, G. Stenberg, T. L. Zhang, W. X. Wan, Y. Wei, X.-D. Wang, L. H. Chai, and J. Zhong (2014), Morphology of magnetic field in near-Venus magnetotail: Venus express observations, *J. Geophys. Res. Space Physics*, *119*, 8838–8847, doi:10.1002/2014JA020461.

Received 1 AUG 2014
Accepted 15 OCT 2014
Accepted article online 18 OCT 2014
Published online 5 NOV 2014

Morphology of magnetic field in near-Venus magnetotail: Venus express observations

Z. J. Rong[1,2,3], S. Barabash[3], Y. Futaana[3], G. Stenberg[3], T. L. Zhang[4], W. X. Wan[1], Y. Wei[1], X.-D. Wang[3], L. H. Chai[1], and J. Zhong[1]

[1]Key Laboratory of Earth and Planetary Physics, Institute of Geology and Geophysics, Chinese Academy of Sciences, Beijing, China, [2]CAS Key Laboratory of Geospace Environment, University of Science and Technology of China, Chinese Academy of Sciences, Hefei, China, [3]Swedish Institute of Space Physics, Kiruna, Sweden, [4]Space Research Institute, Austrian Academy of Sciences, Graz, Austria

Abstract Knowledge of the magnetic field morphology in the near-Venus wake is essential to the studies of magnetotail dynamics and the planetary plasma escape. In this study we use the magnetic field measurements made by Venus Express during the period of April 2006 to December 2012 to investigate the global magnetic field morphology in the near-Venus magnetotail (0–3 Venusian radii, R_V, down tail) in the frame of solar wind electric field coordinates. The hemisphere with electric field pointing toward/away is indicated as ±E hemisphere. It has been reported that the cross-tail field component has a hemispheric asymmetry in the Venusian magnetotail. We report here that this asymmetry should have been formed at the terminator and would transport tailward. In addition, we find that the draped magnetic field lines near both hemispheric flanks are directed equatorward in the region 0–1.5 R_V down tail as it looks like "sinking" into Venus umbra. We estimate the thickness of the magnetotail current sheet and the current density at the sheet center. We find that the average half thickness of central current sheet near +E hemispheric flank (~460 km) is almost twice as thick as that near magnetic equatorial plane (~200 km), but the corresponding current densities at the sheet center are comparable (~6.0 nA/m^2). As a result, the larger cross-tail field component found near the +E hemispheric flank suggests a stronger tailward $\mathbf{j}\times\mathbf{B}$ force, i.e., the more efficient tailward acceleration of plasma in this region, showing the agreement with previous observations of heavy ion outflow from Venus. In contrast, the average magnetic field structure near −E hemispheric flank is irregular, which suggests that dynamic activities, such as magnetic reconnection and magnetic field turbulence, preferentially appear there.

1. Introduction

Many studies have shown that a magnetotail is formed antisunward of Venus [*Phillips and McComas*, 1991, and references therein], although Venus lacks a significant intrinsic dipole moment [*Russell et al*., 1980a]. Earlier Venus explorations, particularly the magnetic field measurements of Pioneer Venus Orbiter in the distant tail region (8–12 Venusian radii, R_V) [*Russell et al*., 1980b], suggest that the Venusian magnetotail is induced when the interplanetary magnetic field (IMF) carried by solar wind, drapes, piles up, and eventually slips around the planet when the solar wind approaching Venus is slowed, compressed, and deflected due to the electric currents in the Venusian ionosphere[e.g., *Russell et al*., 1981; *Dolginov et al*., 1981; *Saunders and Russell*, 1986; *McComas et al*., 1986].

The near-Venus magnetotail (0–3 R_V down tail) has been sampled by several missions to Venus but is not thoroughly explored until the arrival of Venus Express (VEX). VEX, the first European mission to Venus, was launched in November 2005 and went into a highly elliptical and polar orbit around Venus in April 2006 [*Svedhem et al*., 2009]. The orbit period is 24 h with pericenter near the northern terminator, and the average height of pericenter and apocenter are 250 km and 66,000 km, respectively. VEX crosses the magnetotail semiannually (about every four Earth months). Based on VEX measurements, the knowledge of near-Venus magnetotail was advanced and expanded significantly in the past 8 years. Using the magnetic field data measured by Venus Express magnetometer [*Zhang et al*., 2006] during May 2006 to December 2008, *Zhang et al*. [2010] statistically showed that the near-Venus magnetotail is controlled by the IMF orientation as expected if the IMF is draped, and the cross-tail magnetic field component displays a hemispheric asymmetry. The asymmetry shows that the cross-tail component almost has the same polarity sense of external IMF in the hemisphere where the solar wind electric field pointing away from the Venus-Sun line, referred as +E hemisphere usually,

but shows the opposite polarity preferentially in the opposite −E hemisphere. The asymmetry can also be observed in hybrid and multifluid simulations but not in single-fluid MHD simulations [e.g., *Zhang et al*., 2010; *Du et al*., 2013, and references therein; *Jarvinen et al*., 2013]. The true physical reasons are still in debate [*Du et al*., 2013]. The asymmetry may imply that magnetic reconnection can preferentially appear in the −E hemisphere as suggested in some studies [e.g., *Volwerk et al*., 2009; *Zhang et al*., 2012].

The plasma measurements by Analyzer of Space Plasmas and Energetic Atoms (ASPERA-4) [*Barabash et al*., 2007a] onboard VEX demonstrate that there is an escape of planetary ions and the escape channels strongly depend on the magnetotail field structure. Several studies found that the magnetotail plasma sheet is a main channel for the planetary escaping ions [*Barabash et al*., 2007b; *Fedorov et al*., 2008, 2011; *Masunaga et al*., 2013; *Nordström et al*., 2013; *Dubinin et al*., 2013]. The plasma in the +E hemisphere plasma sheet can be accelerated tailward by the draped magnetic field or the $\mathbf{j}\times\mathbf{B}$ force [*Dubinin et al*., 2013].

In addition, morphologically speaking, the scale of Venus-induced magnetosphere is ~1/10 of Earth magnetosphere. In Earth's magnetotail, it is well accepted that various dynamic processes, i.e., magnetic reconnection, flux ropes, and plasma instabilities, occur frequently [e.g., *Baumjohann*, 2002] within the region less than ~30 Earth radii down tail. By the same simple scaling, the equivalent region at Venus would be the near-Venus wake being less than ~3 R_V down tail [*Zhang et al*., 2010]. Therefore, knowledge of the magnetic field morphology in the near-Venus wake is essential to the studies of Venusian magnetotail dynamics and the planetary plasma escape.

This study, following *Zhang et al*. [2010], uses the magnetic field data of VEX between April 2006 and December 2012 to draw the global magnetic field morphology in the near-Venus wake (0–3 R_V down tail). With a larger magnetic field data set than that *Zhang et al*. [2010] used, we are able to derive the 3-D magnetic field morphology in a more extended region, i.e., 0–3 R_V down tail. Note that only the magnetic field component along Sun-Venus line, i.e., B_x, and the cross-tail component, i.e., B_y, are addressed by *Zhang et al*. [2010] within 1.3–3 R_V down tail. We quantitatively estimate the average thickness of central current sheet and the current density at its center. Based on the obtained results, implications for plasma acceleration and escape are discussed.

2. Data and Method

In this paper we use magnetic field data from the magnetometer (MAG) instrument onboard VEX [*Zhang et al*., 2006]. MAG observes three orthogonal components of the magnetic field, and data are sampled at 1, 32, or 128 Hz. The high sampling rates of 128 Hz and 32 Hz are usually used around the pericenter. Later on the ground, all 128 and 32 Hz data are resampled into a 1 Hz data set, which is cleaned with an absolute field accuracy of ~1 nT, and a variable field accuracy better than 0.1 nT [*Zhang et al*., 2006]. To minimize the noise and high-frequency fluctuations, we use a data set with 4 s resolution. Data recorded from April 2006 to December 2012 are used in this study. To identify the bow shock crossing time and location, electron energy spectra from ASPERA-4 [*Barabash et al*., 2007a] are used in addition to MAG data.

Based on the previous Venusian magnetotail studies[e.g., *McComas et al*., 1986; *Zhang et al*., 2010], it is postulated that the IMF controls the magnetic field polarity and orientation in Venusian magnetotail; thus, the used MAG data should be ordered in a frame defined by IMF orientation. However, the IMF strength and orientation generally vary when the spacecraft travels inside the Venusian magnetosphere. Hence, we have to restrict the data to orbits when IMF is steady to understand the morphologic view of Venusian tail. For this, we first determine the location of the bow shock manually by looking at the jump increase of energetic electron density ($E > 20$ eV) from the spectra and the increase of the magnetic field strength as well. Totally, there are 2314 orbits in the time interval considered, and 4628 bow shock crossing locations were obtained. Then, we calculated IMF vectors for each orbit by taking the average 30 min before and after the bow shock crossing. We denote the averaged IMF before the inbound bow shock crossing $\mathbf{B}_1$ and after the outbound crossing $\mathbf{B}_2$. The angle between $\mathbf{B}_1$ and $\mathbf{B}_2$ is defined as α. To consider only the orbit under a steady IMF, we required that $\mathbf{B}_1$ and $\mathbf{B}_2$ satisfy $\frac{2||\mathbf{B}_1|-|\mathbf{B}_2||}{|\mathbf{B}_1|+|\mathbf{B}_2|} < 0.2$ and $\alpha < 30°$. The average (steady) IMF vector is $\mathbf{B} = (\mathbf{B}_1 + \mathbf{B}_2)/2$. Out of 2314 orbits, we find 401 orbits fulfilling the criteria.

Zhang et al. [2010] found that the typical radius of Venusian magnetotail is 1.3 R_V within $0 > X_{VSO} > -3.0\ R_V$. Therefore, in the second step, we confine the magnetotail to be the region $0 > X_{VSO} > -3.0\ R_V$ and

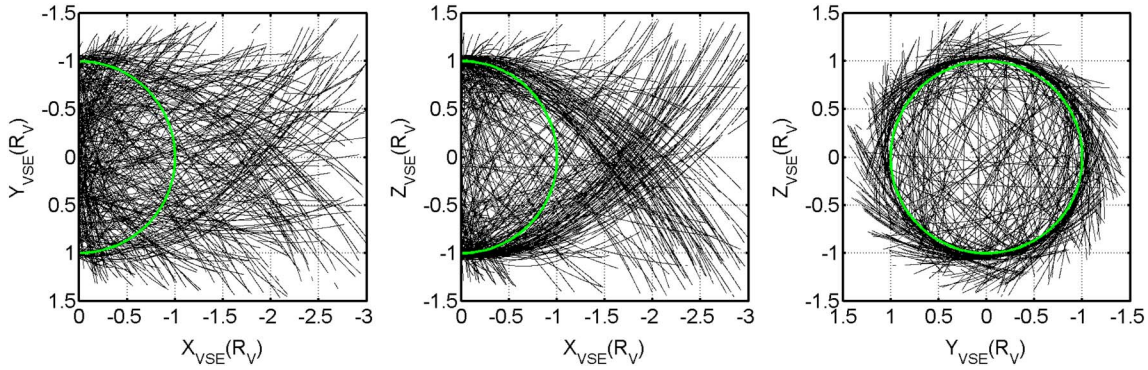

Figure 1. The VEX orbit coverage (398 orbits) of the magnetotail in VSE coordinates. The green line in each of the panels refers to the planetary body.

$\sqrt{{Y_{VSO}}^2 + {Z_{VSO}}^2} \leq 1.3R_V$, where X_{VSO}, Y_{VSO}, and Z_{VSO} are Venus solar orbital (VSO) coordinates (out of 401 orbits, we find 398 orbits crossing tail). In VSO, the *x* axis points to the Sun, the *y* axis points the opposite direction of Venus' orbital motion, and the *z* axis is toward the ecliptic north. Combining the steady IMF requirement with the region of interest, we find 286 orbits crossing the magnetotail. We transform the magnetic field data into Venus solar electric (VSE) coordinates. The VSE coordinates are defined in this way: By considering the average aberration angle of 5° induced by the orbital motion of Venus, the x_{VSE} coordinate is antiparallel to the solar wind flow, the y_{VSE} axis is aligned with the cross-flow component of IMF, and the z_{VSE} axis is aligned with the motional electric field, i.e., in the $-\mathbf{V}\times\mathbf{B}$ direction ($\mathbf{V}$ is the aberrated solar wind flow and $\mathbf{B}$ is the average upstream IMF). In VSE, the hemisphere with electric field pointing toward/away is indicated as ±E hemisphere

In the following sections, the VSE coordinates are used unless otherwise stated. For simplicity, we drop the subscript (VSE) from all coordinates in the VSE frame hereafter.

3. Results

3.1. Average Distribution

Figure 1 shows spatial coverage of the near-Venus magnetotail for the orbits meeting the steady IMF criteria. During April 2006 to December 2012, we find 398 orbits crossing the near tail.

In the VSE frame, the IMF is in the *x-y* plane. The cross-flow component of IMF, i.e., IMF B_y component, is supposedly responsible for the formation of induced magnetosphere, whose dayside part almost vanishes when the IMF becomes parallel or antiparallel to the solar wind flow [*Zhang et al.*, 2009]. Figure 2 shows the histogram of upstream IMF conditions. The left panel gives the IMF B_y, while the right panel gives the

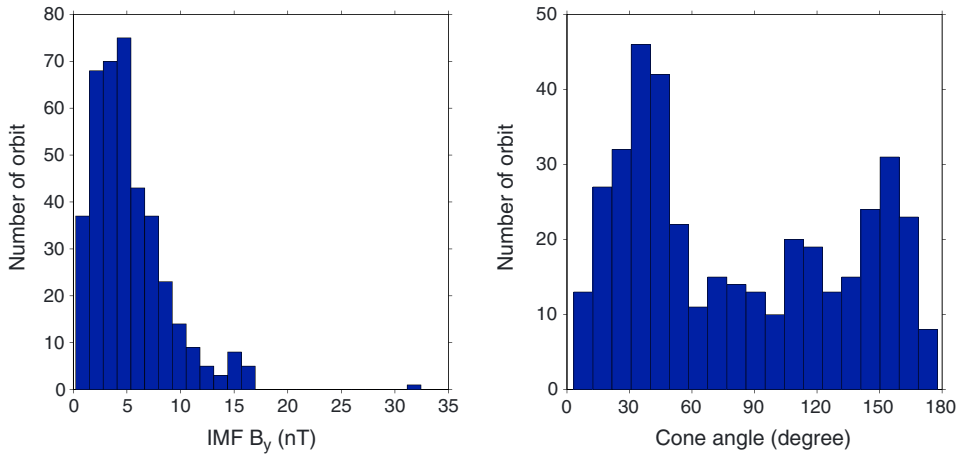

Figure 2. (left) The histogram of the upstream cross-flow component (IMF B_y) in VSE. (right) The histogram of IMF cone angle.

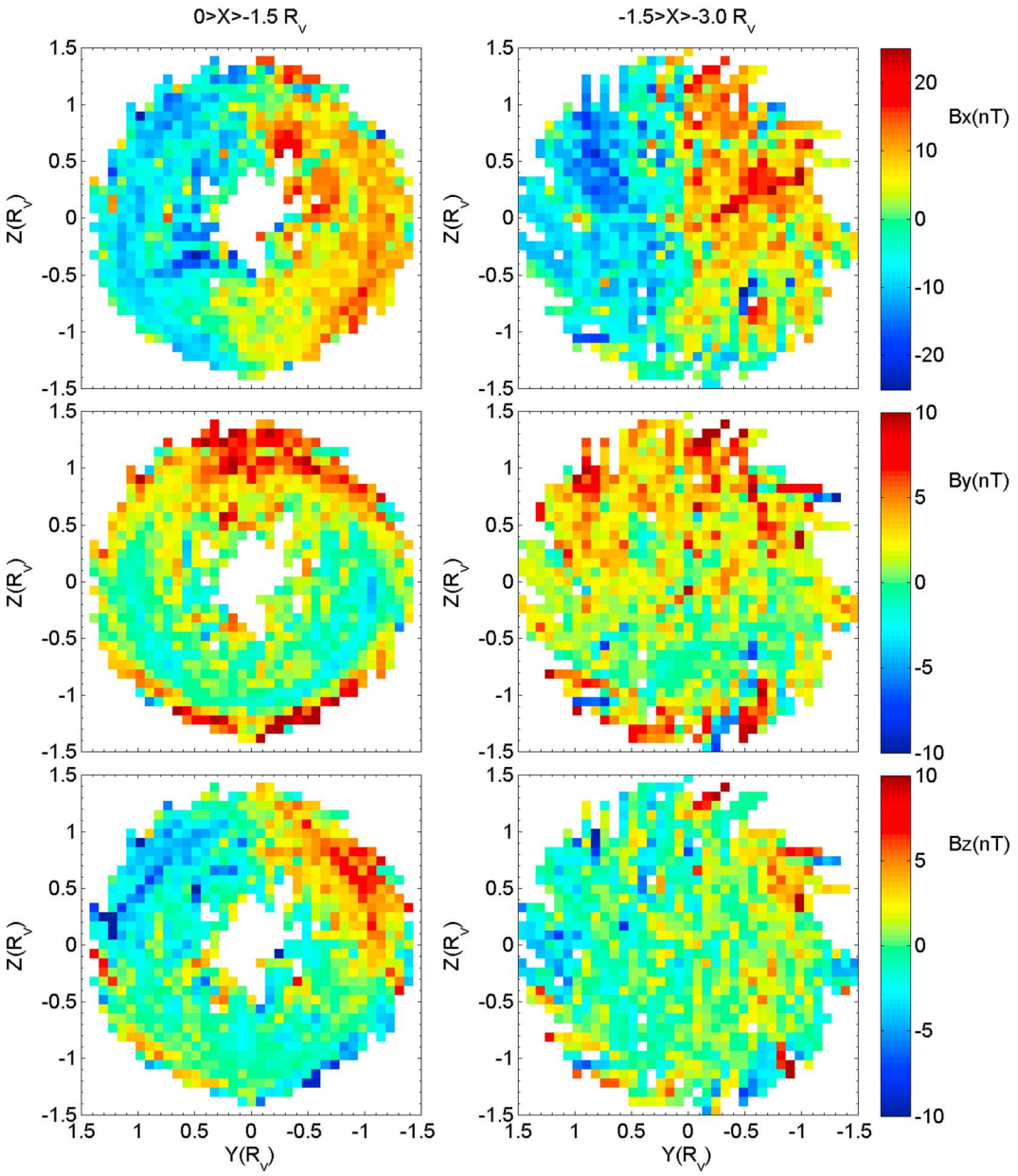

Figure 3. The distribution of magnetic field B_x, B_y, and B_z components in the *y-z* plane for the (left column) inner region ($0 > x > -1.5\ R_V$) and (right column) outer region ($-1.5 > x > -3\ R_V$), as seen from the tail.

histogram of IMF cone angle, which is defined as the angel between the IMF vector and the *x* axis (antiparallel to the average solar wind flow vector). From Figure 2, we note that most tail crossings occurred when IMF $B_y < 10$ nT, and the cone angle peaks at ~35° and ~150°. Using VEX magnetic field measurement in 2007, *Li and Zhang* [2010] reported that the average IMF strength is less than 10 nT and the Parker spiral angle is ~39° at 0.72 AU (Venus orbit). Therefore, the IMF strength and orientations of our data set are good representations of the average IMF condition.

To investigate the spatial variations of magnetotail along the *x* axis, the *x* range is divided into two parts: an inner region $0 > x > -1.5\ R_V$ and an outer region $-1.5 > x > -3.0\ R_V$. The region surveyed by *Zhang et al.* [2010] ($-1.2 > x > -3.0\ R_V$) corresponds to the outer region in this study.

Figure 3 shows the average magnetic field distribution as projected onto the *y-z* plane. To produce Figure 3, we divided the *y-z* plane ($3 \times 3\ R_V$) into 50×50 bins. All observations are put into these bins, and for each bin,

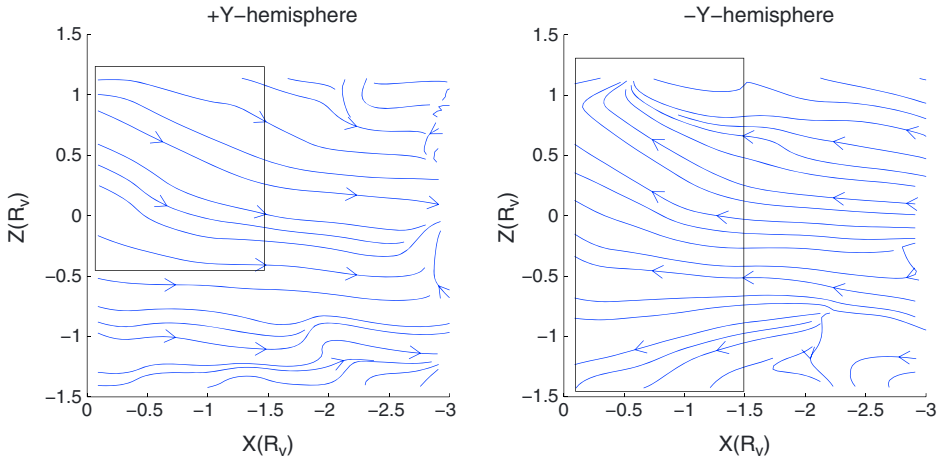

Figure 4. Average magnetic field lines in the *x-z* plane for (left) $y > 0$ and (right) $y < 0$. The rectangles mark the region for the sinking magnetic field lines.

we compute the vector average. The panels from top to bottom show the average of the B_x, B_y, and B_z components, respectively. The left column is for the inner region, while the right column is for the outer region. In the inner region, the hole in the central part of *y-z* plane is due to blockage of the planetary body. The top panels (B_x) show the pattern previously observed by VEX [*Zhang et al*., 2010; *Dubinin et al*., 2013]; that is, the draping of the magnetic field leads to the formation of two tail lobes with opposite magnetic polarities (IMF B_y is always positive). The same pattern had been observed in the distant tail [*Saunders and Russell*, 1986].

Figure 3 (middle row) shows a hemispheric asymmetry in B_y: in the inner region, the B_y component is positive on average and stronger when $z > 0.5\ R_V$ but is weaker and negative when $z < 0.5\ R_V$, and in the outer region, the B_y is positive in almost the entire +E hemisphere ($z > 0$). Previous VEX observations by *Zhang et al*. [2010] noticed the asymmetry in the outer region, and such an asymmetric distribution of B_y has also been observed in the distant tail [*Saunders and Russell*, 1986]. However, no report has been published discussing the tail radial variation of asymmetry. The recent study of *Du et al*. [2013] presented the B_y asymmetric distribution around the terminator region $-0.6 < x < 0.6\ R_V$.

Figure 3 (bottom row) shows the spatial distribution of B_z component. In the inner region, a quadrupole pattern is seen: in +E hemisphere ($Z > 0$), B_z is positive/negative when Y is negative/positive, and the polarity of B_z is reversed in the −E hemisphere ($z < 0$). This quadrupole pattern is not visible in the outer region.

To further investigate the average magnetic field morphology, we plot the streamlines of the magnetic field, i.e., magnetic field lines (MFLs). The MFLs are calculated by an interpolation algorithm and are plotted using the MATLAB software. Figure 4 shows the averaged MFLs computed separately for the two hemispheres $y > 0$ and $y < 0$, respectively. To make the MFLs smoother, the *x-z* plane ($3 \times 3\ R_V$) is divided into 15×15 bins. It is clearly seen from Figure 4 that the MFLs in the inner region are directed toward the *x-y* plane as they look like "sinking" into the Venus umbra, and this is more evident in the +E hemisphere (see the region marked by the rectangular). Here we use the term "sink" to describe the field structure directing toward the equatorial plane, which does not necessarily imply that the field lines are really moving equatorward. This configuration manifests itself as the quadrupole variation of B_z in Figure 3. In the outer region, the MFLs become parallel to the *x-y* plane, and the sinking structure fades away.

Figure 5 shows the MFLs structure in the *x-y* plane. As the same in Figure 4, the *x-y* plane ($3 \times 3\ R_V$) is divided into 15×15 bins to compute the smoother MFLs. To look for a possible variation of the MFL structure along z direction, the surveyed near-Venus magnetotail is divided into three regions: the +E hemispheric flank ($0.5 < z < 1.5\ R_V$), the middle region ($-0.5 < z < 0.5\ R_V$), and the −E hemispheric flank ($-1.5 < z < -0.5\ R_V$). The average MFLs in the three regions are displayed in the three panels of Figure 5. In the +E hemispheric flank and the middle region, the MFLs in the tail are significantly stretched. The MFLs are oriented sunward at $y < 0$ and antisunward at $y > 0$, and the identification of two magnetotail lobes is possible. They are separated by a transition region around $y \sim 0$, usually referred as the current sheet (CS). We note that the MFLs in the

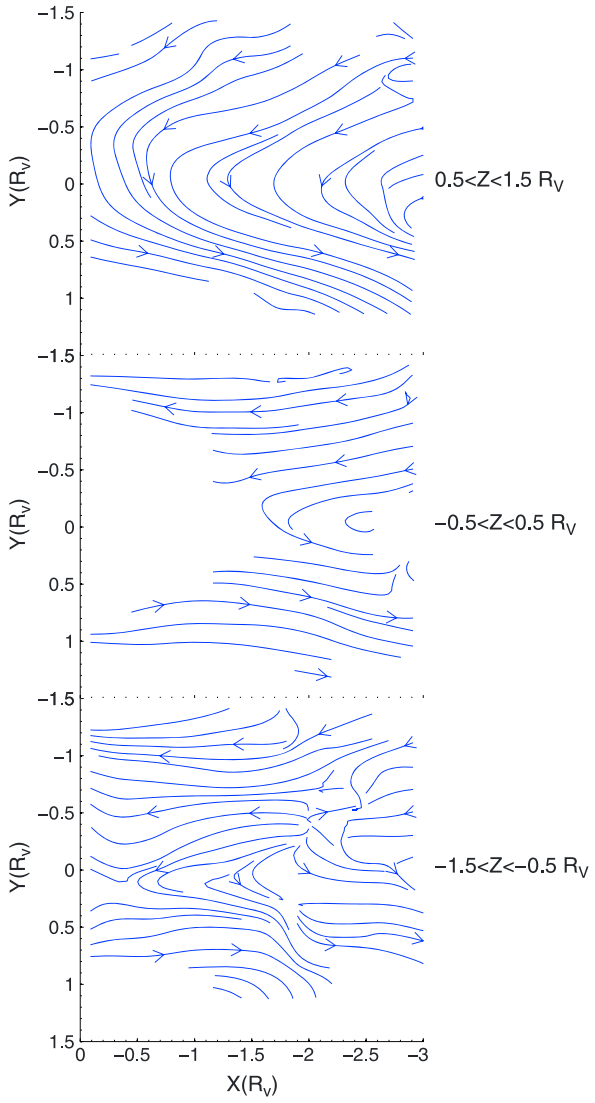

Figure 5. (top to bottom) The structure of magnetic field lines in the *x-y* plane for the +E hemispheric flank ($0.5 < z < 1.5\ R_V$), the middle region ($-0.5 < z < 0.5\ R_V$), and the −E hemispheric flank ($-1.5 < z < -0.5\ R_V$), respectively.

middle region are more stretched than those in the +E hemispheric flank (The B_y component in middle region is on average weaker than B_y in the +E hemispheric flank.) Hence, the CS in middle region is significantly thinner.

In contrast, the MFL structure in −E hemispheric flank is irregular relatively, and no magnetotail lobes can easily be identified particularly for $x < -1.5\ R_V$.

Here we should remind readers that the MFLs we have shown in Figures 4 and 5 are just the representations of averaged magnetic field configuration; they are not the really field lines.

3.2. Characteristics of the Central Current Sheet

In this section, we will quantitatively estimate the current density and thickness of central CS based on the average magnetic field structure shown in Figure 5. Before presenting the estimation, it is necessary to mention the definition of central CS we adopted here. According to the definition of *Shen et al.* [2007], see the Appendix A where the central CS was defined as neutral sheet, the central CS is the region in current sheet where the magnetic field becomes null or is near to the minimum value. Generally, the width of the central CS is much less than that of the corresponding current sheet. The thickness of central CS is defined as the span along the normal direction with B_x changing from $-B_{\mathrm{min}}$ to B_{min}, where B_{min} is the field strength at the CS center ($B_x \sim 0$).

From Figure 5, we observe that the region $-1.5 > x > -2.5\ R_V$ is surveyed sufficiently for the ±E hemispheric flanks as well as the middle region. Moreover, because the sinking effect almost fades away in this region, the MFL plane is nearly parallel to *x-y* plane. Hence, we use data from the region $-1.5 > x > -2.5\ R_V$ to compute the average magnetic field as a function of *y* (the *y* axis is divided into 15 bins for the average calculation). Figure 6 shows the average magnetic field components as functions of *y* for the +E hemispheric flank, the middle region, and the −E hemispheric flank, respectively. The lengths of the error bars are $2\times1.96\frac{\sigma}{\sqrt{n}}$, representing the 95% confidence interval, where $\frac{\sigma}{\sqrt{n}}$ is the standard error of the mean.

For the +E hemispheric flank and the middle region, the B_y component (the cross-tail component) is approximately constant over CS. The B_z component is negligible at the CS center, but at larger *y* values, the quadrupole effect observed in Figure 3 is visible. The B_x component varies significantly over the CS. We fit the B_x component to a Harris sheet model $B_x = B_0 \tanh\left(\frac{y-y_0}{L}\right)$ [*Harris*, 1962], where B_0 is the lobe field, *L* is the typical sheet scale, and y_0 is the shift of sheet center. The fit is shown as a red line in each of the panels in Figure 6, and the fit parameters are given in Table 1. The fits are good except for the overshoots at the CS boundaries.

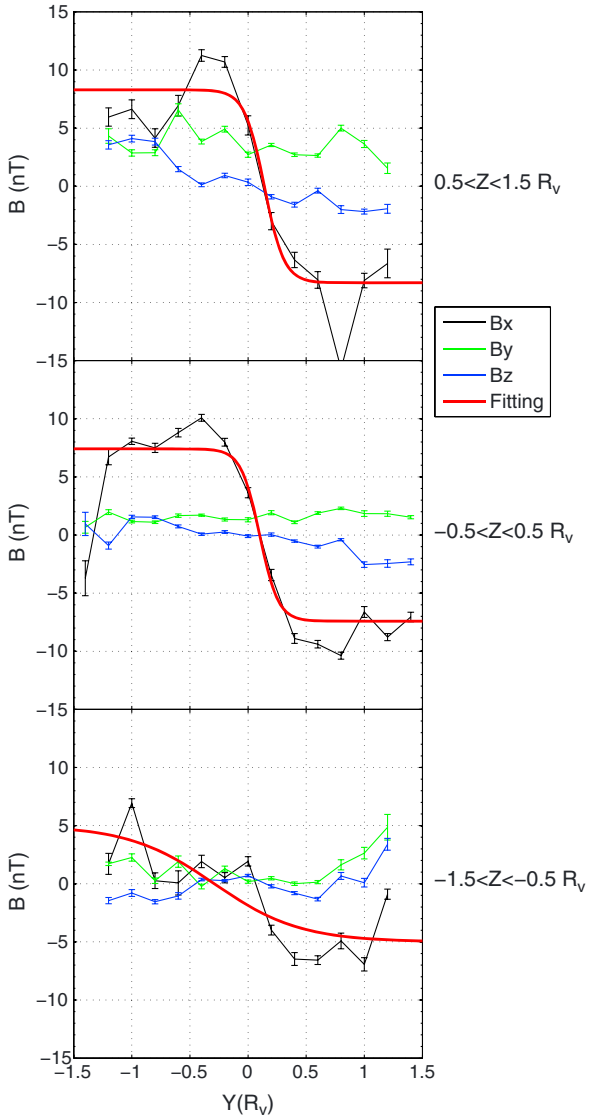

Figure 6. (top to bottom) The averaged magnetic field components as a function of y for the +E hemispheric flank, the middle region, and the −E hemispheric flank within the range $-1.5 > x > -2.5\ R_V$. The B_x component is fitted to a Harris sheet model (red line).

In the −E hemispheric flank, the weaker B_y becomes comparable to B_z around $B_x \sim 0$, and due to the irregular average magnetic field, the Harris model fitting is worse than in the other cases (see the coefficient adjusted R square in Table 1). Since B_y is approximately constant over CS center and B_z is negligible in the +E hemispheric flank and middle region, the CS in there can be considered as a 1-D sheet. The minimum curvature radius of MFLs at CS center can be estimated as $R_{c,\min} = \frac{<B_y>L}{B_0}$ [*Büchner and Zelenyi*, 1989]. $R_{c,\min}$ can represent the half thickness of central CS if CS is 1-D [*Shen et al.*, 2007; *Rong et al.*, 2010]. Table 1 presents the values of $R_{c,\min}$. The current density at CS center, J_0, is computed as $\mu_0^{-1}\frac{dB_x}{dy}\Big|_{y=y_0}$ and tabulated in Table 1. $R_{c,\min}$ and J_0 in the −E hemispheric flank are not given due to the bad fit.

From Table 1, we can see that both L and B_0 are comparable in the +E hemispheric flank and middle region, which necessarily implies the comparable current density J_0 there. However, due to the significant difference of B_y component, the CS in the +E hemispheric flank is more than twice as thick as that near the magnetic equatorial plane.

4. Discussion

We find that close to the planet ($0 > x > -1.5\ R_V$), the strong positive B_y component appears for $z > 0.5\ R_V$, but further out ($-1.5 > x > -3.0\ R_V$), the positive B_y gradually dominates the whole +E hemisphere (see Figure 3 (middle row)). Thus, in view of the radial variation, we suggest that the hemispheric asymmetry of B_y is transported, instead of being created locally. The MFLs, which are directed toward the magnetic equator plane in the range $0 > x > -1.5\ R_V$, would bring the positive B_y component down toward the equator plane as the plasma moves tailward. The original

Table 1. The Estimated Magnetotail Parameters in Different Regions Within $-1.5 > x > -2.5\ R_V$

	$<B_y>$[a] (nT)	$<B_z>$[a] (nT)	y_0[b] (R_v)	B_0[b] (nT)	L[b] (R_v)	$R_{c,\min}$[c] (km)	J_0[c] (nA/m^2)	Adjusted R Square[d]
+E hemispheric flank	3.73	0.08	0.14 ± 0.14	-8.30 ± 2.30	0.17 ± 0.26	460	6.42	0.86
Middle region	1.56	−0.006	0.10 ± 0.17	-7.41 ± 2.28	0.16 ± 0.27	206	6.09	0.79
–E hemispheric flank	0.77	−0.30	-0.29 ± 0.43	-5.00 ± 5.55	0.74 ± 1.70	-	-	0.44

[a]The averaged value over the range $-1.5 < Y < 1.5\ R_V$.
[b]The fitted parameters from Harris sheet model with 95% confidence bounds.
[c]$R_{c,\min}$ and J_0 are the estimated magnetic field curvature radius and current density, respectively, at CS center based on Harris sheet fitting.
[d]The coefficient of adjusted R square indicates the fitting goodness; i.e., the more closer to one it is, the better the fit will be.

asymmetry is then likely associated with a process at the terminator. Consistently, the recent study by *Du et al*. [2013] showed that the evident B_y asymmetry begins within $0 < x < 0.2\ R_V$, where the negative B_y appears in the −E hemisphere. The asymmetry can be reproduced in hybrid and multifluid MHD simulations but not in single-fluid MHD simulations [e.g., *Zhang et al*., 2010; *Du et al*., 2013, and references therein; *Jarvinen et al*., 2013]. (Note, in principle, the radial variation of asymmetry can be yielded in simulations, but it was not addressed exclusively before in the simulation studies.) Recently, *Dubinin et al*. [2014] found that the asymmetry between both hemispheres arises at low altitudes, where friction forces become important. The true mechanisms responsible for the asymmetry are still in debate [*Du et al*., 2013], and we do not intend to discuss it more here. We hope that the radial variation we revealed here can contribute the further simulations to find the true mechanism.

We find that the MFLs in the inner tail region $-0.5 > x > -1.5\ R_V$ are directed toward the magnetic equator plane as they sink into the Venus umbra and that the sinking is more evident in the +E hemisphere. The sinking structure has been noticed previously by *Pérez-de-Tejada* [1986], but in his paper, it is only inferred by one orbit measurements of Pioneer Venus Orbiter. Here we draw it out explicitly from large data set for the first time. The reasons for the sinking MFLs are unclear. *Pérez-de-Tejada* [1986] argued that a viscous interaction between the magnetosheath and the ionospheric plasma heats the magnetosheath plasma and that the heated plasma expands into the nightside pushing the draped magnetic field into the wake. If this argument is right, the expansion should be stronger in +E hemisphere since sinking is more evident there. Here with a rough analysis of $\mathbf{j} \times \mathbf{B}$ force, we could qualitatively reexamine the physical reasons for the sinking. For an initial state without sinking, the tail field structure only consists of B_x and B_y components. The significant variation of B_x component over CS implies a current density component j_z embedding in CS and flowing +E direction. The yielded force component $j_z B_y$ is pointing tailward (we will discuss the related tailward acceleration later), which cannot account for the sinking. The hemispheric asymmetry of B_y component shows increment toward +E direction, which implies a tailward current density component, j_x. The yielded $j_x B_y$ in ±E hemisphere is basically directed ±E direction, because B_y in +E hemisphere is positive, and weaker even negative in −E hemisphere (see Figure 3), which satisfies the orientation of sinking MFLs. However, the B_y asymmetry can be found even in the distant tail [*Saunders and Russell*, 1986], while the sinking MFLs only appears evidently within $0 > x > -1.5\ R_V$. Therefore, the $\mathbf{j} \times \mathbf{B}$ force cannot account for the formation of sinking MFLs. Consequently, the final driving force should be ascribed to the plasma thermal pressure, which shows the consistency with the argument of *Pérez-de-Tejada* [1986]. Further studies exploring the relationship between the plasma flow and the sinking MFLs are needed.

We find that in the region $-1.5 > x > -2.5\ R_V$, the average half thickness of central CS in +E hemispheric flank is ~460 km, which is twice as thick as the estimate for the middle region (~200 km). The variation of half thickness is similar to that found in the Earth's magnetotail, except for the −E hemispheric flank. *Rong et al*. [2011] estimated that the half thickness of central CS in the Earth's magnetotail at a distance 15–19 R_E (Earth radius, $R_E = 6371$ km) down tail is ~0.3 R_E (~2000 km) around the midnight region (equivalent to the middle region) and ~0.8 R_E (~5000 km) in both flank regions. We note that as found on Venus, in the Earth's magnetotail, the central CS at both flanks is just twice as thick as that around midnight region. Meanwhile, the half thickness of central CS in the Earth's magnetotail is almost 10 times thicker than that in the Venus' magnetotail, which demonstrates consistence with the scaling of the two magnetospheres. The thickness of central CS is an important parameter to probe the energetic particle motion in CS. Theoretical studies demonstrated that the particle adiabaticity is determined by $\kappa = \sqrt{R_{c,\min}/\rho_{\max}}$, where $R_{c,\min}$ is the minimum curvature radius of the MFLs or the half thickness of central CS and $\rho_{\max}$ is the maximum gyroradius in central CS. If $\kappa \gg 1$, the particle is magnetized and quasi-adiabatic and vice versa. Some authors [*Büchner and Zelenyi*, 1987, 1989; *Pulkkinen et al*., 1994] have suggested that the onset of the disruption of the current sheet takes place when κ for the electrons in central CS is less than 3. This topic will be addressed further in a future study combining magnetic field and particle measurements.

We find the current density at CS center is ~6.0 nA/m^2 both in the +E hemispheric flank and in the middle region. The cross-tail component, B_y, however, is much larger in the +E hemispheric flank (~3.7 nT) than in the middle region (~1.5 nT). The $\mathbf{j} \times \mathbf{B}$ force is then stronger in the +E hemispheric flank, suggesting a more efficient plasma acceleration tailward, consistent with previous plasma observations [e.g., *Barabash et al*., 2007b; *Fedorov et al*., 2011; *Dubinin et al*., 2013]. It is also interesting to compare our results with the observations

in the distant tail [e.g., *Saunders and Russell*, 1986; *McComas et al*., 1986]. The cross-tail component in the distant tail $-10 > x > -12\ R_V$ [see *Saunders and Russell*, 1986, Figure 17] is comparable to our estimate. Thus, there is no evident radial gradient of magnetic field cross-tail component. The average current density at the CS center in the distant tail ($-8 > X > -12\ R_V$) is ~1.5 nA/m^2 [see *McComas et al*., 1986, Figure 14], compared to our estimate ~6.4 nA/m^2. As a consequence, the tailward ampere force $\mathbf{j}\times\mathbf{B}$ is largest, and the tailward plasma acceleration is most efficient in the +E hemispheric flank of the near-Venus magnetotail if the thermal pressure along X direction is ignored (*McComas et al*. [1986] argued that the assumption is valid because there is no boundary confining the plasma). Assuming the ion of a given specie with a number density of ~0.7 cm^{-3} in the CS, ion would gain the energy ~1.3 keV within a distance of 1 R_V in +E hemispheric flank due to the plasma acceleration by $\mathbf{j}\times\mathbf{B}$.

It is noteworthy that we just adopted the Harris sheet model to fit the statistical spatial profile of B_x component. The Harris model is analytically derived for the 1-D sheet satisfying thermodynamics equilibrium; that is, the model necessarily requires that the normal field component, i.e., B_y, should be ignored and the variation along the z direction should be small compared to that along the y direction or the variation perpendicular to the sheet. However, as we show that a finite B_y component is still existent in CS, and there is an evident field variation of hemispheric asymmetry along the z direction, thus, our application of Harris model fitting is not absolutely strict. The Harris fitting makes sense for the local sheet, where the sheet may locally satisfy the requirement of Harris model. To judge whether a local current sheet in Venusian magneotail is Harris type or not, one has to know the spatial variation of the sheet; that is, the relative velocity of spacecraft to the sheet should be available. The sheet motion is usually assumed to be "frozen" with plasma motion. Nonetheless, because the time resolution for the 3-D ion velocity distribution measured by ion mass analyzer is 192 s [*Barabash et al*., 2007a], while the typical current sheet crossing by VEX is completed within 1–2 min [e.g., *Dubinin et al*., 2013; *Vasko et al*., 2014], the plasma velocity during crossing CS is difficult to be obtained accurately. There is a possible way to check the spatial variation for a given current sheet crossing: if the field temporal variation can be ignored, the sheet is 1-D, and the relative velocity of spacecraft to the normal of current sheet is constant during the crossing; i.e., $\frac{\partial}{\partial t} = 0$ and V_n = const, then the spatial variation of magnetic field can be evaluated by the temporal rate of magnetic field recorded by the spacecraft because of $\frac{d\mathbf{B}}{dt} = V_n\nabla_n\mathbf{B}$. The plot of $\frac{d\mathbf{B}}{dt}$ against B_x would show the spatial variation of magnetic field over the sheet. This idea and application will be detailed in the next research.

We should remind that only the magnetic field data are analyzed in this survey. It is expectable that combining with ASPERA-4 measurements, some topics in magnetotail, e.g., the effect of solar wind dynamic pressure on magnetotail [e.g., *Wei et al*., 2012], the plasma moment distribution, the adiabaticity of charged particles and the current carrier in CS, and the plasma acceleration, could be addressed more in the next studies.

5. Conclusions

Using the VEX magnetic field data during April 2006 to December 2012, we obtain the average magnetic field morphology of the near-Venus magnetotail (0–3 R_V). We confirm the previously observed draping of the magnetic field leading to two magnetotail lobes with opposite magnetic polarities governed by the upstream IMF orientation. We also observe the previously reported hemispheric asymmetry of the B_y component [*Zhang et al*., 2010].We notice that the asymmetry has an evident radial variation; i.e., the positive B_y component mainly appears for $z > 0.5\ R_V$ in the inner region ($0 > x > -1.5\ R_V$) but gradually dominates the whole +E hemisphere ($z > 0$) in the outer region ($-1.5 > x > -3.0\ R_V$). We suggest that the asymmetry is transported tailward, instead of being created locally. The original asymmetry is probably related to a process at the terminator.

We find that the MFLs in the inner tail region $0 > x > -1.5\ R_V$ are directed toward the magnetic equatorial plane as they sink into the Venus umbra. The sinking of MFLs is more evident in the +E hemisphere and fades away in the outer region $-1.5 > x > -3.0\ R_V$. The sinking MFLs may be induced by the convergence of plasma flow toward the nightside as suggested by *Pérez-de-Tejada* [1986].

We find that in the region $-1.5 > x > -2.5\ R_V$, the average half thickness of central CS in the +E hemispheric flank (~460 km) is twice as large as that half thickness estimated for the middle region (~200 km), which are nearly 10 times as thin as that in the Earth's magnetotail with distance 15–19 R_E down tail showing the consistence with the scaling of the two magnetospheres.

The estimated current density at the CS center is ~6.0 nA/m^2 in both the +E hemispheric flank and in the middle region. The cross-tail component, B_y, however, is much larger in the +E hemispheric flank (~3.7 nT) than in the middle region (~1.5 nT). Hence, a stronger tailward $\mathbf{j} \times \mathbf{B}$ force suggests a more efficient plasma tailward acceleration in the +E hemispheric flank, consistent with the observations [e.g., *Barabash et al.*, 2007b; *Fedorov et al.*, 2011; *Dubinin et al.*, 2013]. Comparisons with observations in the distant tail showed that the plasma acceleration tailward is most efficient in the +E hemispheric flank of the near-Venus magnetotail.

Acknowledgments

The data for this paper are available at ESA's Planetary Science Archive (ftp://psa.esac.esa.int/pub/mirror/VENUS-EXPRESS/). The authors are thankful to the VEX MAG team for providing the magnetic field data and to the APSERA-4 team for providing the plasma data. This work is supported by the Chinese State Scholarship Fund (201304910018), Chinese Academy of Sciences (KZZD-EW-01-2), the National Key Basic Research Program of China (2011CB811405), the National Natural Science Foundation of China grants (41104114, 41374180, 41321003, and 41131066), and the CAS Key Laboratory of Geospace Environment, University of Science and Technology of China.

Michael Liemohn thanks the reviewers for their assistance in evaluating this paper.

References

Barabash, S., et al. (2007a), The analyzer of space plasmas and energetic atoms (ASPERA-4) for the Venus Express mission, *Planet. Space Sci.*, *55*, 1772–1792.

Barabash, S., et al. (2007b), The loss of ions from Venus through the plasma wake, *Nature*, *450*, 650–653, doi:10.1038/nature06434.

Baumjohann, W. (2002), Modes of convection in the magnetotail, *Phys. Plasmas*, *9*, 3665–3668, doi:10.1063/1.1499116.

Büchner, J., and L. M. Zelenyi (1987), Chaotization of the electron motion as the cause of an internal magnetotail instability and substorm onset, *J. Geophys. Res.*, *92*, 13,456–13,466, doi:10.1029/JA092iA12p13456.

Büchner, J., and L. M. Zelenyi (1989), Regular and chaotic charged particle motion in magnetotaillike field reversals: 1. Basic theory of trapped motion, *J. Geophys. Res.*, *94*(A9), 11,821–11,842, doi:10.1029/JA094iA09p11821.

Dolginov, S. S., E. M. Dubinin, E. G. Eroshenko, P. L. Izrailevich, I. M. Podgorny, and S. I. Shkolnikova (1981), Field configuration in the magnetospheric tail of Venus, *Kosmicheskie Issledovaniia*, *19*, 624–633.

Du, J., C. Wang, T. L. Zhang, and E. Kallio (2013), Asymmetries of the magnetic field line draping shape around Venus, *J. Geophys. Res. Space Physics*, *118*, 6915–6920, doi:10.1002/2013JA019127.

Dubinin, E., M. Fraenz, T. L. Zhang, J. Woch, Y. Wei, A. Fedorov, S. Barabash, and R. Lundin (2013), Plasma in the near Venus tail: Venus Express observations, *J. Geophys. Res. Space Physics*, *118*, 7624–7634, doi:10.1002/2013JA019164.

Dubinin, E., M. Fraenz, T. L. Zhang, J. Woch, and Y. Wei (2014), Magnetic fields in the Venus ionosphere: Dependence on the IMF direction—Venus express observations, *J. Geophys. Res. Space Physics*, *119*, 7587–7600, doi:10.1002/2014JA020195.

Fedorov, A., et al. (2008), Comparative analysis of Venus and Mars magnetotails, *Planet. Space Sci.*, *56*, 812–817.

Fedorov, A., S. Barabash, J.-A. Sauvaud, Y. Futaana, T. L. Zhang, R. Lundin, and C. Ferrier (2011), Measurements of the ion escape rates from Venus for solar minimum, *J. Geophys. Res.*, *116*, A07220, doi:10.1029/2011JA016427.

Harris, E. G. (1962), On a plasma sheet separating regions of oppositely directed magnetic field, *Nuovo Cimento*, *23*, 115–121, doi:10.1007/BF02733547.

Jarvinen, R., E. Kallio, and S. Dyadechkin (2013), Hemispheric asymmetries of the Venus plasma environment, *J. Geophys. Res. Space Physics*, *118*, 4551–4563, doi:10.1002/jgra.50387.

Li, X. Y., and T. L. Zhang (2010), Statistics of the interplanetary magnetic fields observed at 0.72 AU and 1 AU, *Chin. J. Space Sci.*, *30*(4), 356–361.

Masunaga, K., Y. Futaana, G. Stenberg, S. Barabash, T. L. Zhang, A. Fedorov, S. Okano, and N. Terada (2013), Dependence of O + escape rate from the Venusian upper atmosphere on IMF directions, *Geophys. Res. Lett.*, *40*, 1682–1685, doi:10.1002/grl.50392.

McComas, D. J., H. E. Spence, C. T. Russell, and M. A. Saunders (1986), The average magnetic field draping and consistent plasma properties in the Venus magnetotail, *J. Geophys. Res.*, *91*, 7939–7953, doi:10.1029/JA091iA07p07939.

Nordström, T., G. Stenberg, H. Nilsson, S. Barabash, and T. L. Zhang (2013), Venus ion outflow estimates at solar minimum: Influence of reference frames and disturbed solar wind conditions, *J. Geophys. Res. Space Physics*, *118*, 3592–3601, doi:10.1002/jgra.50305.

Pérez-de-Tejada, H. (1986), Distribution of plasma and magnetic fluxes in the Venus near wake, *J. Geophys. Res.*, *91*(A7), 8039–8044, doi:10.1029/JA091iA07p08039.

Phillips, J. L., and D. J. McComas (1991), The magnetosheath and magnetotail of Venus, *Space Sci. Rev.*, *55*, 1–80, doi:10.1007/BF00177135.

Pulkkinen, T., D. Baker, D. Mitchell, R. McPherron, C. Huang, and L. Frank (1994), Thin current sheets in the magnetotail during substorms: CDAW 6 revisited, *J. Geophys. Res.*, *99*(A4), 5793–5803, doi:10.1029/93JA03234.

Rong, Z. J., C. Shen, A. A. Petrukovich, W. X. Wan, and Z. X. Liu (2010), The analytic properties of the flapping current sheets in the earth magnetotail, *Planet. Space Sci.*, *58*(10), 1215–1229, doi:10.1016/j.pss.2010.04.016.

Rong, Z. J., W. X. Wan, C. Shen, X. Li, M. W. Dunlop, A. A. Petrukovich, T. L. Zhang, and E. Lucek (2011), Statistical survey on the magnetic structure in magnetotail current sheets, *J. Geophys. Res.*, *116*, A09218, doi:10.1029/2011JA016489.

Russell, C. T., R. C. Elphic, J. G. Luhmann, and J. A. Slavin (1980a), On the search for an intrinsic field at Venus, Proc. Lunar Planet. Conf., 11th, 1897–1906.

Russell, C. T., R. C. Snare, J. D. Means, and R. C. Elphic (1980b), Pioneer Venus Orbiter fluxgate magnetometer, *IEEE Trans. Geosci. Remote Sens.*, *GE-18*, 32–36.

Russell, C. T., J. G. Luhmann, R. C. Elphic, and F. L. Scarf (1981), The distant bow shock and magnetotail of Venus: Magnetic field and plasma wave observations, *Geophys. Res. Lett.*, *8*, 843–846, doi:10.1029/GL008i007p00843.

Saunders, M. A., and C. T. Russell (1986), Average dimension and magnetic structure of the distant Venus magnetotail, *J. Geophys. Res.*, *91*, 5589–5604, doi:10.1029/JA091iA05p05589.

Shen, C., X. Li, M. Dunlop, Q. Q. Shi, Z. X. Liu, E. Lucek, and Z. Q. Chen (2007), Magnetic field rotation analysis and the applications, *J. Geophys. Res.*, *112*, A06211, doi:10.1029/2005JA011584.

Svedhem, H., D. Titov, F. Taylor, and O. Witasse (2009), Venus Express mission, *J. Geophys. Res.*, *114*, E00B33, doi:10.1029/2008JE003290.

Vasko, I. Y., et al. (2014), The structure of the Venusian current sheet, *Planet. Space Sci.*, *96*, 81–89, doi:10.1016/j.pss.2014.03.013.

Volwerk, M., et al. (2009), Substorm activity in Venus's magnetotail, *Ann. Geophys.*, *27*, 2321–2330.

Wei, Y., et al. (2012), A teardrop-shaped ionosphere at Venus in tenuous solar wind, *Planet. Space Sci.*, *73*, 254–261, doi:10.1016/j.pss.2012.08.024.

Zhang, T. L., et al. (2006), Magnetic field investigation of the Venus plasma environment: Expected new results, *Planet. Space Sci.*, *54*, 1336–1343, doi:10.1016/j.pss.2006.04.018.

Zhang, T. L., J. Du, Y. J. Ma, H. Lammer, W. Baumjohann, C. Wang, and C. T. Russell (2009), Disappearing induced magnetosphere at Venus: Implications for close-in exoplanets, *Geophys. Res. Lett.*, *36*, L20203, doi:10.1029/2009GL040515.

Zhang, T. L., W. Baumjohann, J. Du, R. Nakamura, R. Jarvinen, E. Kallio, A. M. Du, M. Balikhin, J. G. Luhmann, and C. T. Russell (2010), Hemispheric asymmetry of the magnetic field wrapping pattern in the Venusian magnetotail, *Geophys. Res. Lett.*, *37*, L14202, doi:10.1029/2010GL044020.

Zhang, T. L., et al. (2012), Magnetic Reconnection in the Near Venusian Magnetotail, *Science*, doi:10.1126/science.1217013.